Generation of focused electron beam and x-rays by pyroelectric and photogalvanic crystals

N. Kukhtarev, T. Kukhtareva, M. Bayssie, J. Wang, J. Brownridge, et al.

N. Kukhtarev, T. Kukhtareva, M. Bayssie, J. Wang, J. D. Brownridge, V. Rotaru, "Generation of focused electron beam and x-rays by pyroelectric and photogalvanic crystals," Proc. SPIE 6023, Tenth International Conference on Nonlinear Optics of Liquid and Photorefractive Crystals, 60230G (6 December 2006); doi: 10.1117/12.648199

SPIE.

Event: Tenth International Conference on Nonlinear Optics of Liquid and Photorefractive Crystals, 2005, Alushta, Ukraine

Generation of focused electron beam and X-rays by pyroelectric and photogalvanic crystals

N.Kukhtarev, T.Kukhtareva, M.Bayssie, J.Wang
Physics Department, Alabama A&M University, nkukhtarev@aamu.edu

J.D.Brownridge
Department of Physics, Applied Physics and Astronomy
State University of New York at Binghamton, Binghamton, New York 13902-6000, USA

and V.Rotaru
Physics Department, Moldova State University. Kishinev, Moldova

ABSTRACT

We have developed a model to explain the phenomena of electron focusing by pyroelectric and photogalvanic crystals. The pyroelectric crystals used to compare experiments with theory were Fe doped and un-doped $LiNbO_3$. The crystals were either heated from the +z end or illuminated with a laser (to test photogalvanic effect). Heating the crystals by passing a current through a resistor attached to the +z end produced the pyroelectric effect: a change in polarization in response to a change in temperature. Illuminated with a CW solid–state diode pumped laser (532 nm, 100 mW) produces the photogalvanic effect: the build up of charge on the polar surfaces of the crystal. In both cases the polar ends of the crystal becomes electrically charged and produced self-focusing electron beams that were imaged on a ZnS screen. Using different targets we have produced X-rays, and demonstrated X-ray imaging of metal masks.

Keywords: pyroelectric crystal, photogalvanic effect, self-focusing

1. INTRODUCTION

The observations of an interesting phenomena, the generation of a self-focused electron beam by pyroelectric crystals was recently reported by J. D. Brownridge and S, M. Shafroth [1]. A cylinder shape $LiNbO_3$ crystal was used to generate high energy (160 keV) nearly monoenergetic electrons beams [2,3]. The generation of electrons was explained qualitatively by the appearance of uncompensated [4] charges on the polar -z faces of the crystal during the cooling part of the thermal cycles to which the crystal was subjected [5]. In a vacuum environment uncompensated charge is produced as the spontaneous polarization increase with decreasing temperature, this occurs during both uniform and non-uniform temperature changes [6]. For the results reported here the temperature changes were non-uniform [2]. A uniform change in temperature of 75 °C in a $LiNbO_3$) will result in a spontaneous polarization change ΔP_s of 0.015 C/m^2 on the surface of a z-cut crystal [7]. For a non-uniform change in temperature ΔP_s will be <0.015 C/m^2. The strength of electric field on the surface of the crystal will be $|E_0| = 1.35 \times 10^7$ V/cm [7,8]. Over time, however, $|E_0|$ will decrease to zero as the polarization change is compensated or neutralized by charge from the environment. Ionization of the residual gas in the vacuum chamber is the source on the compensating or neutralizing charge.

Just how these crystals produce the self-focusing electron beams have not been explained. However, they have been used to produce compact crystal X-ray generators [9]. In this paper, we present an explanation of the electron beam focusing phenomena by pyroelectric crystals and demonstrate ability of X-ray generation and X-ray imaging. We also describe other experiments with photogalvanic crystals[10] where we have observed similar electron-beam focusing phenomena

Tenth International Conference on Nonlinear Optics of Liquid and Photorefractive Crystals,
edited by Gertruda V. Klimusheva, Andrey Iljin, Sergey Al. Kostyukevych, Proc. of SPIE Vol. 6023,
60230G, (2005) · 0277-786X/05/$15 · doi: 10.1117/12.648199

2. Model of electron beam focusing by charged crystals

We hypothesized that the main mechanism of electron beam focusing is due to the formation of uncompensated charges at the surface of the crystal. During the heating-cooling cycle, electrical charge in and on the face of the crystal will be non-uniformly distributed. This occurs in part because of the temperature gradient within the crystal. The crystal was heated from one end with a resistor and the other end is exposed to the vacuum. A non-uniform distribution of charge creates non-uniform electric fields near the surface of the crystal, which may in turn, produce the focusing effect. A detailed calculation of temperature and charge distribution requires solutions to heat and electric field equations. When we consider heat equations for crystals in the shape of rods, or the shape of a slab, it can be shown that a temperature gradient exists when a crystal is heated from one end while the other end is exposed to a dilute gas in a vacuum. Thus, this T-gradient may lead to the non-uniform distribution of charge needed for focusing of electrons. From laser physics it is well known that laser rods heat up during operation and that a radial gradient of temperature is produced in the rods. This temperature gradient is responsible for focusing a generated photon (laser) beam [11]. This is a useful analogy suggest that photons and electrons may behave in a similar way in geometric-optics approximation.

Recently, the generation of high electrical fields in the ferroelectric crystals, due to the photogalvanic effect was reported [19]. The illumination of Fe-doped $LiNbO_3$ crystals leads to photo generation of a steady-state current that is mainly directed along the polar axis. This photogalvanic current produces a voltage buildup on the surface of the crystal [4]. Its magnitude is limited by ionization of ambient gas or by high voltage breakdown at the surface of the crystal. Photogalvanic voltage as high as 10^2 kV has been observed in previous experiments [12,13] both in the volume of the crystal and on the surfaces. The photogalvanic effect, and the pyroelectric effect, both produce high electric fields at the surfaces of these crystals. Likewise, subsequent discharges may generate current pulses [10]. In several experiments it has been shown that these electrical pulses in photogalvanic crystals could be used to power electro-optic modulators [10].

The generation of Bremsstrahlung radiation was recently observed from photogalvanic crystals at atmospheric pressure. We expect that when a photogalvanic crystal is placed in a moderate vacuum, it will also generate characteristic X-rays from metal targets and from the crystal itself. The main difference between these effects is that the pyroelectric effect is transient and the photogalvanic effect can be observed in the steady-state (DC illumination), or with pulsed illumination. Another important difference is the physical origin of the charge. The photogalvanic effect primarily generates charge from ionization of the impurities in the crystal. In contrast, the primary source of charge in the pyroelectric crystal is the polarization charge produced when the temperature of the crystal is changed. Also, pyroelectric crystals produced secondary charge when ambient gas is ionized by the uncompensated polarization charge.

Pyroelectric and photogalvanic effects can generate high voltages in and on the surface of crystals. Accordingly, we will discuss a possible mechanism for electron beam focusing by these crystals. An "electrostatic lenses" is suggested for both types of crystals. Two different geometries will be considered, a plane cut crystal and cylindrical cut crystal (cylinder axis is along the polar axis). For both geometries we will assume that charge is distributed only on the crystal edges. This simplified model will allow us to begin explaining the focusing effect. More detailed calculations that take into account charge distribution over the entire crystal will be provided in future publications.

2.1. Model for a plane crystal (a-cut).

We will consider geometry introduced in Fig.1. The heat equation for the crystals temperature T and the equation for pyroelectric current may be written as:

$$\frac{dT}{dt} = D\Delta T + q$$
$$\frac{dP}{dt} + \frac{P}{\tau} + \varepsilon_0 \varepsilon \frac{dE}{dt} + \sigma E = J + \alpha \frac{\Delta T}{\tau} \qquad (1)$$

Here D is the thermal diffusivity, q = Q/(Cp m), Q is the heat flux, m is the crystal mass, Cp is the specific heat, ε_0 is the dielectric constant for vacuum, ε is the material dielectric constant, P is the normal component polarization density, σ is conductivity, J is the total current, α is a pyroelectric coefficient. The electric field E may be found from the Poisson equation.

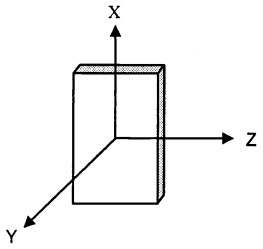

Fig. 1. A schematic diagram of the planer crystal used to produce the electron beam (line) shown in the Fig. 6(b). A $LiNbO_3$ crystal was cut to the dimension X = 21mm, Y = 2mm and Z = 10mm.

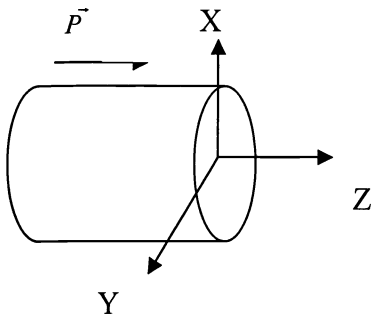

Fig. 2. A schematic diagram of the cylindrical crystal used to produce the image shown in Fig. 6(a). A $LiNbO_3$ crystal was ground into a cylinder 4mm in diameter and 10mm long. The polar axis is along Z as shown in the schematic diagram.

The total current may have components related to plasma formation near the crystal surface and to field emission from the crystal.
For a wide thin crystal plate (crystal Y-directions are much bigger than thickness in X-direction), heat equation becomes one-dimensional and in the steady-state has solution

$$T(x) = To - qx^2/(2D) \qquad (2)$$

Here, the boundary conditions T(0) = To and dT/dx = 0 at x=0. If we assume that conductivity is negligible and current J is small, then the polarization change δP will be proportional to temperature change δT, in a steady state condition,

$$\delta P = \alpha \delta T \qquad (3)$$

This polarization change is equivalent to the appearance of the surface charge density
and equal to δP.
We have observed that the heating-cooling cycles of the crystal lead to the generation of non-uniform temperature and polarization charge distribution in the crystal. To get an approximate analytical solution for the electrical potential and electric field created by this non-uniform charge redistribution, we will further simplify the problem.
We will assume that only the crystal edges are charged and the rest of the crystal surface is neutral (z = 0, where z is along the polar axis). Formally, this indicates that we substituted a quadratic term in equation (2) for x^s, where s is a large even number.

This approach is similar to approximation of a real potential wall by a box-type potential in quantum mechanics. With this approximation, we may then analytically calculate the potential φ and the electrical field $E_x = -\frac{\partial \varphi}{\partial x}$. Our goal is to show that E_x will have distribution that will allow us to explain focusing of charged particles. Direct calculation of the potential φ distribution created by charges along the crystal edges (with linear density ρ_e) gives:

$$\varphi = \frac{\rho_e}{2\pi\varepsilon_0} \ln\left(\frac{4y^2{}_0}{r_1 r_2}\right) \tag{4}$$

here $r_{1,2} = (z^2 + (x \pm \frac{d}{2})^2)^{1/2}$, ε_0 – is the dielectric constant in the vacuum. The potential (4) was received using the assumption that y-extension of this crystal $2y_o$ is much larger than d

$\varphi_\infty \to 0$ when $y_0 \to \infty$

Electric field's components $E_x = -\frac{\partial \varphi}{\partial x}, E_z = -\frac{\partial \varphi}{\partial z}$ follow from (4)

$$E_x = \frac{\rho_e x(x^2 + z^2 - (\frac{d}{2})^2)}{2\pi\varepsilon_0 (r_1 r_2)^2} \text{ and } E_z = \frac{z\rho_e}{2\pi\varepsilon_0}\left(\frac{1}{r^2{}_1} + \frac{1}{r^2{}_2}\right) \tag{5}$$

We can see from the equation (5) and Figs. 3-5 that electrons will be experiencing the focusing force in the vicinity of the crystal surface, where electron coordinate X, Z satisfy relation

$$x^2 + z^2 \le (\frac{d}{2})^2 \tag{6}$$

Outside this area electrons will be accelerated away from the central plane (x=0). In other words, electrons will experience focusing transversal force (~E_x) near the crystal surface Z=0. Equations of motion for electrons will be

$$\frac{d^2x}{dt^2} + \alpha_x \frac{dx}{dt} = \frac{E_0 ed}{m} \frac{x(x^2 + z^2 - (\frac{d}{2})^2}{r_1^2 r_2^2}$$

$$\frac{d^2z}{dt^2} + \alpha_z \frac{dz}{dt} = \frac{E_0 ed}{m} z\left(\frac{1}{r_1^2} + \frac{1}{r_2^2}\right) \tag{7}$$

here $E_0 \equiv \frac{\rho_e}{2\pi\varepsilon_0 d}$

$\alpha_{x,z}$ are damping constants for the motion along X and Z direction

2.2. Model for the cylinder crystal

Correspondingly, for the cylinder geometry (Fig.2), end heating of the crystal will lead to a quadratic-type radial non-uniform distribution of temperature and polarization charge. In the case of photogalvanic crystal, illumination of the surface of the crystal by a laser beam creates charge spots on the surface due to photogalvanic current. These charges (photo-induced electrons) will diffuse from the laser-spot center, forming negatively charged rings on the crystal surface. Analytically speaking, we again assume that only the circular edges are charged with the charge density ρ_e. Direct calculation of the potential distribution φ in the general point M(x,0,z) lying in the plane XZ leads to the integral

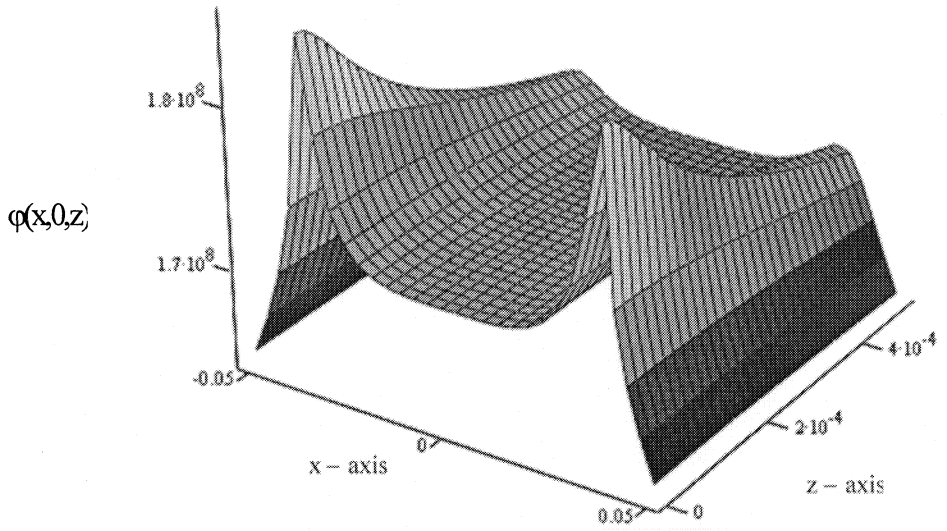

Fig. 3 The potential distribution φ(x,z), (Volt) near the crystal surface plotted x-axis, (m) as the width of the crystal and z-axis (m) distance from the surface of the crystal.

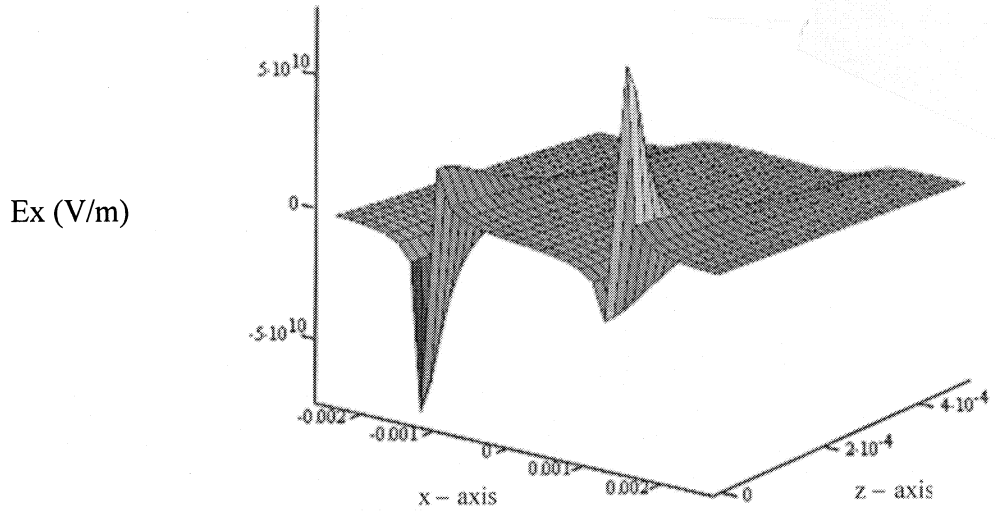

Fig. 4. Distribution of Electrical Field, E_x near crystal surface along the width, x-axis and away from crystal surface in z-axis, (m).

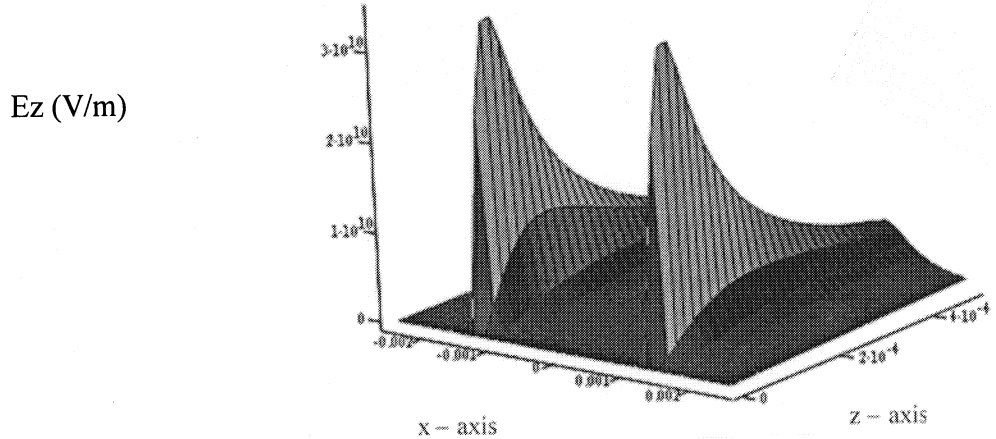

Fig. 5. Distribution of Electric Field, E_z field near the crystal surface along the width, x-axis and away from crystal surface in z-axis (m).

$$\varphi(x,0,z) = \frac{\rho_e}{4\pi\varepsilon_0}\int_0^{2\pi}\frac{a d\Phi}{\sqrt{A - B\cos\Phi}} \tag{8}$$

where $A \equiv x^2 + z^2 + a^2$, $B = 2xd$.

General solution for Eq. (8) leads to the elliptic integrals, and is not easily analyzed. The solution will be greatly simplified by assuming, that $\left|\frac{B}{A}\cos\Phi\right| << 1$

$$\begin{aligned}\varphi(x,0,z) &= \frac{a\rho_e}{2\varepsilon_0\sqrt{A}}(1+\frac{3}{16}\frac{B^2}{A^2}) \\ E_z &= \frac{d\rho_e z}{\varepsilon_0 A^{3/2}}[1+\frac{15x^2d^2}{4A^2}]\end{aligned} \tag{9}$$

The electric field E_x will be:

$$E_x = -\frac{\partial\varphi}{\partial x} = \frac{a\rho_e x}{2\varepsilon_0 A^{5/2}}[(x^2+z^2) - \frac{d^2}{2}] \tag{10}$$

Comparing the results for the plane and cylindrical crystal (Eqs. (5) and (10)) we can see similarity. For the cylinder crystal the focusing area is bounded by relation:

$$x^2 + z^2 \le \frac{d^2}{2} \tag{11}$$

this specifies that the beam will be focused at distances $z \ge a$ from the crystal surface.

The equations of the motion for electrons near the cylindrical crystal will be:

$$\begin{aligned}\frac{d^2x}{dt^2} + \beta_x\frac{dx}{dt} &= E_0\frac{\pi e a^2}{m}\frac{x[(x^2+z^2) - \frac{d^2}{2}}{A^{5/2}} \\ \frac{d^2z}{dt^2} + \beta_z\frac{dz}{dt} &= E_0\frac{\pi e d^2}{m}\frac{z}{A^{3/2}}[1+\frac{3x^2d^2}{2A}]\end{aligned} \tag{12}$$

here $\beta_{x,z}$ are the damping constants for the movement along x and z directions.

3. Experiments and results.

3.1 Pyroelectric effect.

From a large z cut lithium niobate ($LiNbO_3$) crystal purchased from Crystal Technology, Inc., several smaller crystals were fashioned. Some into round cylindrical crystals (Fig. 2) of varying lengths from 2mm to 10mm long and from 4mm to 6mm in diameter and one into a rectangular shape of 2.5mm thick, 15.9 mm wide and 10 mm long (Fig. 1). The polar axis is solely the z-axis as shown in Figs. 1 and 2. A 62-ohm wire wound resistor (the heater) was epoxied to the +z end of each crystals using J B Weld epoxy. A type K thermocouple was attached to the crystal at the resistor/crystal junction to monitor the temperature. The crystals were electrically floating.

To produce the focused beams shown in Fig. 6 and in reference 14 the +z base of the crystals was heated to ~160 °C from about ~20 °C in a stable pressure environment of less than about 1 mTorr and let cool to room temperature by removing power from the heater. When the +z base of a crystal is heated to ~160 °C the beam begin forming as the temperature fall through about 90 °C and usually become stable as the temperature fall through about 50 °C [2]. There is nothing-unique about 160 °C or 50 °C, what is important is that there is a change in temperature of the crystal from some

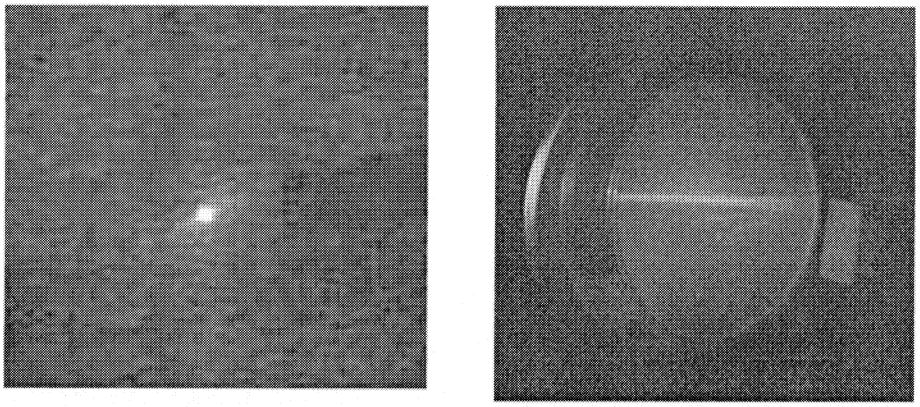

(a) (b)

Fig. 6 (a) Photograph of the electron beam image at the focal length, ~21mm for a 4 mm diameter x 10 mm long $LiNbO_3$ crystal. A ZnS screen was used to image the beam. The residual gas is N_2 and the pressure is about 1 mTorr. The temperature of the crystal is about 35 °C and falling. (b) Photograph of the electron beam (line) imaged on a ZnS screen as electrons are accelerated away from a plane crystal that is 2mm thick, 21mm wide and 10mm long (the z-axis). Notice that fluorescent line on the ZnS is perpendicular to the long (21mm) plane of the crystal.
(b) Electron beam imaged on a ZnS screen as electrons are focused and accelerated away from a plane crystal.

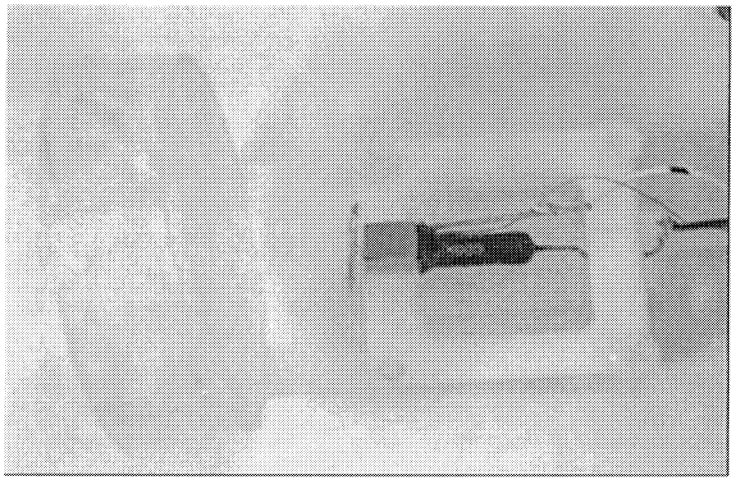

Fig.7. Photograph of Ce:Fe: $LiNbO_3$ attached to the heater and fluorescence ZnC screen. The copper-sticker mask has been glued to the ZnC screen to produce X-ray imaging

initial temperature and then return to approximately that initial temperature. The initial temperature may be at any temperature between about 14K to about 500K [15].

In Fig. 6 (a) we show the results of heating the +z base of a 10mm long 4mm diameter crystal of a $LiNbO_3$ to about 160 °C and returning it to about 20 °C at a pressure of 1.0 mTorr in N_2 gas. The crystal is at a distance of 21mm from a ZnS screen used to image the beam. At a distance of 21mm the beam spot is at its smallest, we call this the focal point [1]. In Fig. 6(b) we show the results of heating the +z base of the 2mm thick, 21 mm wide and 10 mm long crystal of $LiNbO_3$ to about 160 °C and returning it to about 20 °C at a pressure of 2.0 mTorr in N_2 gas. Here the electrons are "focused" into a line that is rotated 90° with respect to a plane that is parallel to the thinnest dimension of the crystal. A ZnS screen was used to image the line. The distance between the crystal and the ZnS screen was about 25mm. There is a clear correlation between the shape of the crystals and the electron beam image produced on the ZnS screen.

For the X-Ray generation we introduced K-Cl and Cu targets between the crystal and X-Ray detector and observed characteristic spectra (Fig.8,9). To demonstrate ability of X-Ray imaging with pyroelectric crystals (Fig.7) we have used metal mask (copper sticker-electrodes), 1mm thick, that were attached to the sealed commercial dental film (for intra-oral use). On the Fig.10 we can see very clear picture of two copper letters, which was done after about 5 exposures to heating-cooling cycles. In addition, pronounced dark spot appear in the center, that demonstrate strong focusing effect during transient process of electron beam induced X-Ray generation. Dental film integrate in time X-Ray flux and allow to observe in one experiment both focusing and imaging ability. From the shadow-type character of X-Ray image, we can conclude, that X-Ray generation was from the dental film envelope and shielding cover.

3.2 Photogalvanic effect.

We use Fe-doped LiNbO3 crystals to produce the photogalvanic effects in this paper.

A typical crystal is z cut and is about 3mm thick (alone the z axis) and about 10mm in diameter. The crystal was placed in a vacuum chamber (pressure 1- 30 mTorr) and illuminated with a CW solid–state diode pumped laser (532 nm, 100 mW) through a glass window. We observed the glow on the ZnS screen caused by electrons striking the screen (Fig.11). The screen was at a distance of about 15 mm from the crystal. When the pressure in the chamber was gradually increased, a bright "focused" spot was observed on the ZnS screen. As the pressure continued to raise the spot disappeared a lightning-type flashes, a high voltage discharge or breakdown. This lightning-type flashes is observed during a rise in pressure when the pyroelectric effect is employed, see the Video clip in reference 14.

We measured a temperature increase in the crystal during laser illumination from 25 °C to 35 °C after 15 minutes of illumination. A 10°C change in the temperature of the crystal will not generate electrons with enough energy to fluorescent the ZnS screen. However, when a Fe-doped crystal of $LiNbO_3$ is heated from about 25°C to about 140°C a fluorescent spot is produced on a ZnS screen. This is a clear indication that laser-induced heating alone cannot explain the high-energy electrons generated during laser illumination. Instead, these results indicate, that the laser-illuminated Fe-doped crystal of $LiNbO_3$ produce electron beams via the photogalvanic effect. The photogalvanic effects is, however, similar to that observed when the crystal is heated to a much higher temperature with a resistive heater attached to one end.

4. Discussion and conclusion

We have found that edge-charged crystals have a tendency to focus charged particles; negatively charged crystal focus electrons. Solving simple problems evolving the propagation of electrons from the surface of the crystal by assuming average $\langle E_x \rangle$ and $\langle E_z \rangle$, the field focusing distance for electron that originated at the edge of the cylindrical crystal will be defined by relation (initial speed is 0).

$$Z_f = \frac{d}{\sqrt{2}} \frac{\langle E_z \rangle}{\langle E_z \rangle}$$

Fig. 9. X-ray generation during the heating cycle (21^0C-125^0C
Fig .10. Kukhtarev et al, SPIE Proceeding

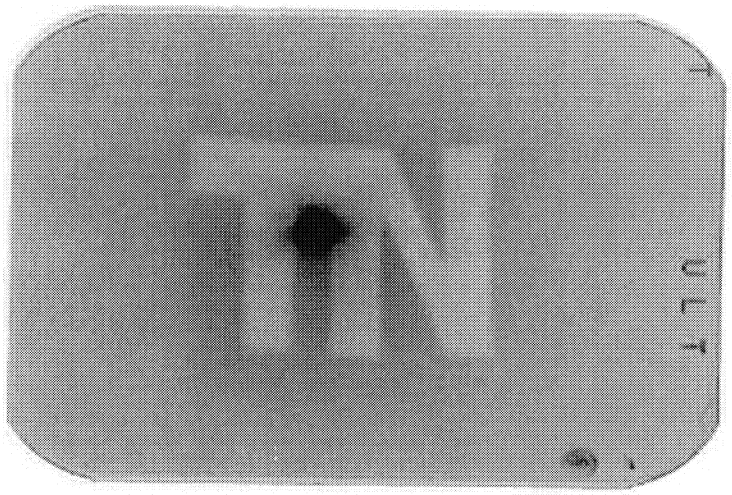

Fig. 10. X-Ray imaging of the copper mask using commercial dental film

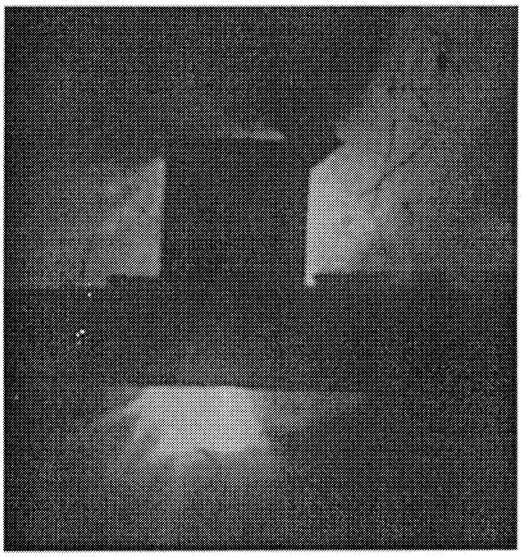

Estimating $\langle E_x \rangle$ as E_x at x ~a/2, z~d/4, and $\langle E_z \rangle$ as $E_z \approx \frac{\rho_e dz}{2\varepsilon_0 (a^2 + z^2)^{3/2}}$ at $z \approx a/2,\ x = 0$ can get for the focus distance:

$$Z_{foc} = 5d$$

These results compare with the experimental data on the pyroelectric crystals. We have demonstrated ability of X-Ray imaging of the metal mask' using commercial dental film.

Our preliminary experiments with photogalvanic crystals show that the focused electron beam may be produced by illumination of Fe-doped $LiNbO_3$ crystals with a CW solid–state diode pumped laser (532 nm, 100 mW). The crystals placed in a moderate vacuum where a high electrical field is generated via photo-induced migration of electrons, liberated by light from the impurity centers. We expect that laser illuminated photogalvanic crystal will generate X-ray in a manner similar to doped and un-doped pyroelectric crystals. This will allow the extension of the range of possible modes of operations and applications for the compact crystal X-ray generator.

ACKNOWLEGEMENT

This work has been done by support of Title III program of Alabama A&M University and CRDF grant (award number ME2-2317-CH-02) We thank S. M. Shafroth for useful discussion and continued interest, and Dr. Akira Ueda, Fisk University in Nashville, TN for the help with the vacuum chamber, Dr. T.Hudson for providing lithium niobate crystal, and Dr. D.Booth for providing X-ray films.

REFERENCES

1. J. D. Brownridge and S. M. Shafroth, Appl. Phys. Lett., vol. **79**, pp.3364–3366, Nov. 2001.
2. J. D. Brownridge and S. M. Shafroth, Appl. Phys. Lett., vol. **83**, pp.1477–1479, Aug. 2003.
3. J. D. Brownridge, S. M. Shafroth, D. W. Trott, R. B. Stoner, and W. M. Hook, Appl. Phys. Lett., vol. **78**, pp. 1158–1159, Feb. 2001.
4. G. I. Rozenman, Sov. Phys. Solid State **30** (1240), 1988.
5 J. D. Brownridge and S. Raboy, J. Appl. Phys., vol. **86**, pp. 640–647, Jul. 1999.
6. R. S. Weis and T. K. Gaylord, Appl. Phys. vol. **37**, pp. 191–203, 1985
7. B. Rosenblum, P. Braunlich and J. P. Carrico, Appl. Phys. Lett. 25, **17** (1974)
8. V. S. Kortov K. K. Shvarts, A. F. Zatsepin, A. I. Gaprindashvili, A. V. Guilbis and Z. A. Grant, Sov. Phys. Solid State **21**(6), 1093 (1979)
9. http://www.amptek.com./coolx.html
10. N. Kukhtarev, T. Kukhtareva, E. Edwards, B. Penn, D. Frazier, H. Abdeldaem, P.P. Banerjee, T. Hudson and W.A. Friday, Journal of Nonlinear Optical Physics &Materials, **V. 11**, No. 4(2002) 445-453.
11. M. Innocezi, H. Yura, et al " Thermal modeling of continuous-wave end-pumped solid-state laser" Appl. Phys. Lett., **V. 56(19),** pp.1831-33, 1990.
12. N. Kukhtarev S. Lyuksyutov, P. Buchhave, T. Kukhtareva, K. Sayano, P. Banerjee. Phys. Rev.A, **V. 58**, No.5, 1051 (1998)
13. V. Obuchovsky, V. Lemeshko Sov.Tech. Phys. Lett. (11), 573 (1986), Proc.SPIE 2795, 185 (1995)
14. J. D. Brownridge, Video clip, Dynamical Behavior of Beam as Pressure Increases Available at: http://www.binghamton.edu/physics/brownridge.html.
15 J. D. Brownridge and S. Raboy, Preprint at http://www.arxiv.org/ftp/cond- mat/papers/0205/0205189.pdf